



## Designed self-assembly of metamaterial split-ring colloidal particles in nematic liquid crystals

Journal:	<i>Soft Matter</i>
Manuscript ID	SM-ART-04-2019-000842.R1
Article Type:	Paper
Date Submitted by the Author:	31-May-2019
Complete List of Authors:	Aplinc, Jure; University of Ljubljana Faculty of Mathematics and Physics, Department of Physics Pusovnik, Anja; University of Ljubljana Faculty of Mathematics and Physics, Department of Physics Ravnik, Miha; University of Ljubljana, Faculty of Mathematics and Physics



Cite this: DOI: 10.1039/xxxxxxxxxx

## Designed self-assembly of metamaterial split-ring colloidal particles in nematic liquid crystals

Jure Aplinc,<sup>a</sup> Anja Pusovnik,<sup>a,\*</sup> and Miha Ravnik<sup>a,b</sup>

Received Date

Accepted Date

DOI: 10.1039/xxxxxxxxxx

www.rsc.org/journalname

The fabrication of orientationally and positionally ordered colloidal clusters is of interest to several fields from material science to photonics. An interesting possibility to obtain such colloidal crystalline structures is by the self-assembly of the colloidal particles in a liquid crystal matrix. This work demonstrates the self-assembly in nematic liquid crystal of a specific type of colloidal particles – the split ring resonators (SRR), which are well known in the field of photonic metamaterials and chosen for their ability to obtain resonances in the response of magnetic field. Using free energy minimisation calculations, distinctly, we optimise the specific geometrical parameters of the SRR particles to reduce and prevent formation of irregular metastable colloidal states, more generally, using concepts of pre-designed self-assembly. Using the pre-designed particles, we then show self-assembly into two- and three-dimensional nematic colloidal crystals of split-ring particles. Our work is a contribution to the development of designed large-scale colloidal crystals, the properties of which could be finely tuned with external parameters, and are of high interest for photonic applications, specifically as tunable metamaterials.

### 1 Introduction

Liquid crystals are capable materials for the orientational and positional ordering of colloidal particles, i.e. the self-assembly<sup>1–5</sup>. For a colloidal particle of some general shape introduced in the nematic, a rise in the free energy of the system appears due to the elastic deformation of the nematic field surrounding the particle, as caused by the orientational profile imposed at the particle surface. It has been shown<sup>6,7</sup> that the preferred orientation of the particle, together with the defects that form around the particle, can induce not only orientational but also positional self-assembly of the particles, leading to particle chains<sup>8–10</sup>, two-dimensional<sup>11,12</sup> and three-dimensional colloidal crystals and assemblies<sup>13–17</sup>. Recent research points in the direction of discovering the role of the geometry of colloidal particles<sup>18–20</sup>, also studying the multipolar nature of the elastic interaction between colloidal particles in liquid crystals<sup>21–23</sup> and coarse-grained treatment of nematic colloids<sup>24</sup>.

The three-dimensional, large-scale colloidal crystals with long-range order are, amongst other, interesting in the field of photonic applications<sup>25–28</sup>. The periodic structures on the scale smaller than wavelength can be used to efficiently alter the properties of the propagating light wave – performing as metamaterials<sup>29–31</sup> –,

in particular the transmission and polarization properties<sup>26,32–35</sup>. By using liquid crystals, the birefringence of the material can be used to exhibit control over the flow-of-light at the wavelength scale. Additionally, by applying external fields on the liquid crystal or changing the temperature, one can control the effective refractive index of the composite<sup>36,37</sup>.

A distinct geometry of interest in view of photonic metamaterial applications is the split-ring-resonator (SRR) shape. This specific shape is appealing due to the significance of the SRR particle: the circular shape of the SRR produces a magnetic dipole when illuminated with light of the appropriate frequency, and is thus capable of generating a resonance in the effective magnetic response  $\mu_{eff}$  of the structure<sup>30</sup>. In combination with long conductive rods, which produce a resonance in the effective electric response<sup>38</sup>, so that for a certain region of incoming wavelengths both the effective permittivity  $\epsilon_{eff}$  and permeability  $\mu_{eff}$  were negative, the SRRs were the first particle shape with which negative refractive index was realized<sup>39</sup>. A self-assembled SRR material would make a capable tool in controlling the flow-of-light. Additionally, such materials could be made photonically well tunable if using optically tunable surrounding medium, such as nematic liquid crystals<sup>40</sup>.

In this article, we demonstrate the designed self-assembly of split ring colloidal particles in nematic into 2D and 3D colloidal crystals, for potential use as optical metamaterials. Firstly, we design a single SRR horseshoe particle, where we focus on the approach to avoid formation of (irregular) metastable states –

<sup>a</sup> Faculty of Mathematics and Physics, University of Ljubljana, Jadranska 19, Ljubljana, Slovenia.

<sup>b</sup> Jožef Stefan Institute, Jamova 39, Ljubljana, Slovenia.

\* E-mail: anja.pusovnik@fmf.uni-lj.si

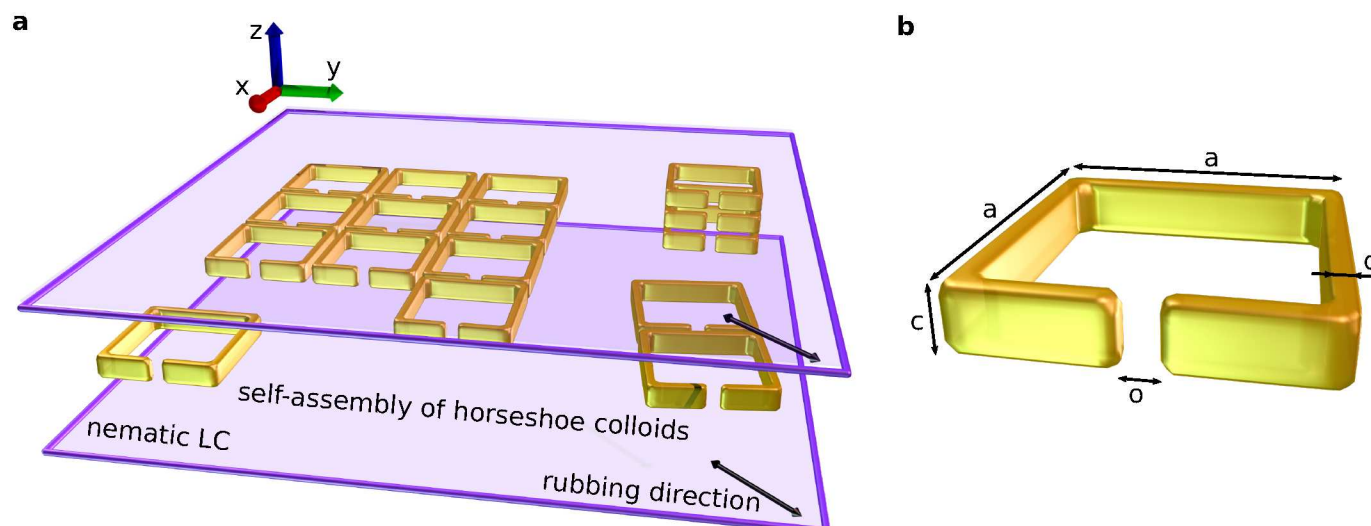


**Fig. 1** Scheme of self-assembly of horseshoe colloids in nematic liquid crystal. (a) Schematic depiction of horseshoe colloid self-assembly into 1D, 2D and 3D colloidal crystals within the nematic cell with strong uniform planar anchoring on the surfaces (black arrow, sketched in  $xy$ -plane). (b) The geometrical parameters of horseshoe colloids, that are used for geometrical optimisation.

that form regularly in nematic colloids but are not desired for photonic applications –, using geometric optimisation of particle shape. Specifically, we design horseshoe particles that exhibit higher-symmetry rotational ordering and inter-particle potentials, despite the overall complex horseshoe shape of individual particle. Using optimised particles, we then show formation of 2D and 3D nematic colloidal crystals from SRR particles, which are of high relevance for potential use as metamaterials. Distinctly, we show the structure of reduced nematic degree of order region within the split ring, that is of primary relevance for tuning in metamaterial applications. More generally, the goal of this work is towards the realisation of soft and tunable metamaterials, in notable distinction to current state-of-the-art usually solid metamaterials.

## 2 Methodology and shape optimisation

For design of regular nematic colloidal structures (2D and 3D colloidal crystals), we use combination of numerical free energy minimisation and particle shape optimisation, as explained below. Distinctly, this requires a rather substantial set of numerical calculations, in our case of the order of few 1000 individual full free energy minimisations, each for different geometry or material parameters, which then have to be jointly analysed in view of optimisation of selected material properties.

### 2.1 Free energy minimisation

A strong method for studies of nematic colloidal structures is the Landau-de Gennes (LdG) free energy approach<sup>41</sup>. It is based on the full tensorial order parameter field  $Q_{ij}$ , which incorporates the orientation of the director  $\mathbf{n}$ , orientation of the possible biaxial ordering relative to the director, scalar degree of order  $S$  and biaxiality  $P$ . LdG modelling is a phenomenological approach which uses a tensor order parameter to construct a free energy functional  $F$ , which is used to fully characterise the nematic colloidal

dispersion material. We use one elastic constant approximation for the LdG free energy:

$$\begin{aligned}
 F = & \int_{\text{LC}} \left\{ \frac{A}{2} Q_{ij} Q_{ji} + \frac{B}{3} Q_{ij} Q_{jk} Q_{ki} + \frac{C}{4} (Q_{ij} Q_{ji})^2 \right\} dV \\
 & + \int_{\text{LC}} \left\{ \frac{L}{2} \frac{\partial Q_{ij}}{\partial x_k} \frac{\partial Q_{ij}}{\partial x_k} \right\} dV \\
 & + \int_{\text{Surf}} \left\{ \frac{W}{2} (\tilde{Q}_{ij} - \tilde{Q}_{ij}^\perp)^2 \right\} dS,
 \end{aligned} \quad (1)$$

where LC denotes the integration over the bulk of the liquid crystal and *Surf* over the surface of the colloidal particles. The first line accounts for the variation of the nematic degree of order;  $A$ ,  $B$  and  $C$  are material parameters. The term in second line penalises elastic distortions of the nematic, where  $L$  is the elastic constant. The term in third line in  $F$  accounts for the nematic ordering imposed by the surface of the colloidal particle (i.e. surface anchoring). We assume planar degenerate anchoring with  $W$  being the anchoring strength. The auxiliary tensors  $\tilde{Q}_{ij}$  and  $\tilde{Q}_{ij}^\perp$  respectively denote the  $Q$ -tensor with added trace and its projection to the surface, as defined by Fournier and Galatola<sup>42</sup>. The total free energy  $F$  is minimised numerically by using an explicit Euler relaxation finite difference scheme on a cubic mesh<sup>43</sup>. In the calculations of the binding free energies of periodic 2D and 3D colloidal structures (sections 3.2 and 3.3), we assume that the overall crystal is finite and surrounded by a region of (sufficiently large) non-distorted homogeneously aligned nematic, which allows to compare free energies of unit cells of different volume (upon properly accounting for the Landau bulk free energy).

In calculations, we use the material parameters of typical nematic liquid crystal:  $L = 4 \times 10^{-11}$  N,  $A = -0.172 \times 10^6$  Jm<sup>-3</sup>,  $B = -2.12 \times 10^6$  Jm<sup>-3</sup>,  $C = 1.73 \times 10^6$  Jm<sup>-3</sup>, and the strength of the planar degenerate anchoring at the particle surfaces  $W = 10^{-2}$  Jm<sup>-2</sup>. The simulations were performed on a square grid consist-

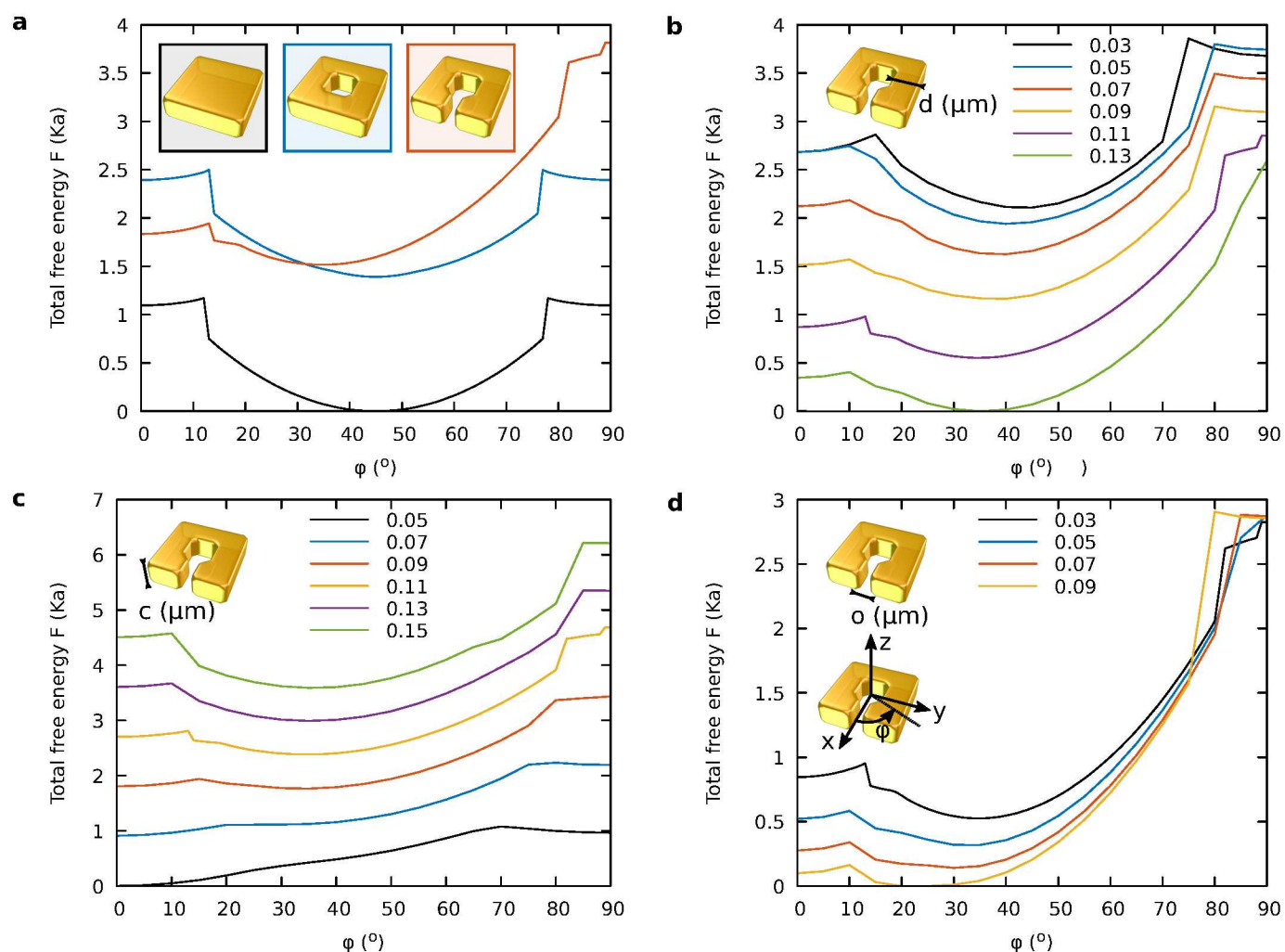


**Fig. 2** Shape and geometry optimisation of the horseshoe colloidal particle. (a) Free energy of the colloidal particle in the shape of a square, square with hole and horseshoe for different angles relative to the undistorted far-field nematic director. Asymmetry in the particle design causes shift of minimum, indicating likely proneness for self-assembly into irregular structures. The dimensions of horseshoe are  $a = 0.3 \mu\text{m}$ ,  $c = 0.1 \mu\text{m}$ ,  $d = 0.1 \mu\text{m}$  and  $o = 0.03 \mu\text{m}$ . Dependence of the total free energy on (b) horseshoe frame thickness  $d$ , (c) particle thickness  $c$ , and (d) slit width  $o$ . The values of the varied geometrical parameters are given in insets in  $\mu\text{m}$ . Free energy is measured in units of  $Ka$ , where  $a$  is the size of the particle and  $K$  is the single Frank elastic constant:  $K = 9LS_{eq}^2/2 = 5.1 \times 10^{-11} \text{J/m}$ , with  $S_{eq} = 0.53$ . Note that the volume of the LC is different for different particle geometries and sizes, with calculations performed in a simulation box of fixed size.

ing of  $200 \times 200 \times 120$  points (single horseshoe colloidal particle), or less (2D and 3D colloidal crystal). The geometry of the colloidal particles studied in this article varies; however, to give general sense of dimensions, a notable set of analysis is done with horseshoe particles of dimensions  $a = 0.5 \mu\text{m}$ ,  $c = 0.1 \mu\text{m}$ ,  $d = 0.05 \mu\text{m}$  and  $o = 0.03 \mu\text{m}$  and  $a = 0.3 \mu\text{m}$ ,  $c = 0.05 \mu\text{m}$ ,  $d = 0.1 \mu\text{m}$  and  $o = 0.03 \mu\text{m}$  (as noted in Fig. 1b). Note that mesh spacing in our simulations is  $\Delta x = 10 \text{ nm}$ .

## 2.2 Optimisation of particle shape

The main parameters that control the self-assembly of colloidal structures in nematics are the geometry and the surface anchoring. We consider particles with strong planar degenerate anchoring on the surfaces, immersed in the nematic liquid crystal with homogeneous far field orientation, which is determined by planar anchoring on the cell walls (Fig. 1a). Given the notably complex

horseshoe-like shape of the particle – as needed for applications in photonic metamaterials<sup>44</sup> –, in general, different pathways for the self-assembly are expected, leading to different regular, or more likely irregular, (meta)stable particle structures<sup>45–47</sup>, unless using approaches for assisting self assembly, such as with optical tweezers<sup>48–50</sup>, other external light fields<sup>51</sup>, boundary conditions<sup>52</sup>, or chemical and photo-patterning<sup>53,54</sup>. For photonic applications, usually regular (periodic or quasi-periodic) structures are required to achieve homogenised material response. Our idea here is to geometrically (similarly could very likely be achieved also by designing surface anchoring profiles) optimise the particle shapes according to all their geometrical parameters, preserving their overall horseshoe shape, but reduce their tendency to form irregular structures, by symmetrising their nematic distortion profile. Note that we optimise the particles manually, by observing the minima in the profiles of the free energy, but it would

be interesting to develop/implement automated algorithms or methodologies for such geometrically optimised approach to the pre-designed self-assembly in complex fluids.

Figure 2a shows the free energy of nematic cell containing particle in shape of a square, a square with a hole and a horseshoe for different relative angle  $\varphi$  between the particle and undistorted far-field nematic director (as imposed by top and bottom cell surfaces. Angle  $\varphi$  is defined in the inset of Fig. 2d). The square particle and square particle with hole are mirror-symmetric with respect to the particle diagonal. Therefore, the free energy is also symmetric and minimal when the particle is oriented at an angle  $45^\circ$  with respect to the far-field director. This configuration minimises the regions of reduced nematic degree of order (defect regions), which are the main contributors to the free energy. The square hole in the particle causes additional defects to appear within the hole and thus raises the free energy. With additional opening in the wall – i.e. creation of the slit – the horseshoe particle accommodates even a further distortion region, which increases the free energy even further. More importantly, introducing the slit breaks the diagonal mirror symmetry of the particle with respect to the far-field director, which causes the shift of the minimum in free energy to angles around  $30^\circ$ , which is direct indication that in any self-assembly of multiple particles multiple structures are likely to emerge.

Varying the geometrical parameters of the horseshoe affects the position of the minimum of free energy. Figure 2b shows the dependence of the free energy on the frame thickness  $d$ , for all other geometrical parameters of the horseshoe kept constant. For large thickness of the frame  $d$  the minimum shifts towards smaller angles  $\varphi$ , while smaller  $d$  shifts the minimum towards  $45^\circ$ . By decreasing the height  $c$  of the horseshoe (Fig. 2c), the local minimum shifts towards  $45^\circ$ , however decrease of the height also introduces the global minimum at  $0^\circ$  when height  $c < 0.11 \mu\text{m}$ . The opening in the horseshoe  $o$  effectively represents the degree of asymmetry, therefore the minimum shifts away from the symmetric case at  $45^\circ$  when the opening is increased (Fig. 2d). According to minimisation curves for individual particles shown in Fig. 2, we choose two particle designs that have symmetric alignment with respect to far field for consideration for self-assembly. Type-1 particle preferentially aligns at angle  $\varphi = 45^\circ$  and type-2 particle aligns along the far-field direction. The specific ratios of the geometrical parameters are:  $a : c : d : o = 5 : 1 : 0.5 : 0.33$  for type-1 particles and  $a : c : d : o = 3 : 1 : 1 : 0.33$  for type-2 particles. Topologically, the nematic profiles of both type-1 and type-2 particles exhibit surface defect regions -i.e. regions of reduced nematic degree of order-, which are generalisation of surface boojums, that generally emerge at surfaces with planar anchoring<sup>20,55,56</sup>. The topological invariants (such as charge) of nematic defects are determined by the topology of the particles where strictly topologically, the horseshoe-particles are genus 0 objects, i.e. equivalent of spheres. However, as the slit only very locally distorts the nematic profile, one might also consider the emergent nematic defects from the perspective of torus (handlebody) geometry<sup>18,57</sup>.

The aligning properties of particles 1 and 2 are investigated further with free energy analysis of the single particle free energy for arbitrary direction of the particle relative to the far field ne-

matic director given by particle orientation angles  $\varphi$  and  $\theta$  (see Fig. 3a; black arrow indicates the direction of the undistorted far-field nematic director). Figures 3b and c show the free energy of single type-1 and type-2 particles immersed in nematic liquid crystal and positioned in the centre of the simulation box; the far-field homogeneous alignment is set by fixed boundary conditions at the walls of the simulation box. The free energy of type-1 particle experiences a strong minimum when  $\varphi = 45^\circ$ ,  $\theta = 90^\circ$  (Fig. 3b) which means that the far-field director field lies in the plane of the particle, diagonally to the edges as shown in Figure 3d. The topological defects form at the edges of the horseshoe and in the slit. The defects in the slit are shown with the zoom-in in the inset. The director field in the slit is asymmetric because of the tilted alignment of the horseshoe regarding the far-field director within the  $xy$  plane. The isosurfaces showing regions of reduced degree of order (red) are drawn for nematic degree of order  $S = 0.39$  (Fig. 3d). The free energy of the type-2 particle has a strong minimum at  $\varphi = 0^\circ$ ,  $\theta = 90^\circ$  (Fig. 3c), which means that the far-field director lies in plane of the particle, such that it is aligned with the slit (Fig. 3e). The surface nematic defects form in the vicinity of the surfaces where the planar alignment is in conflict with the surrounding director field orientation. The zoom in of the director field in the slit is shown in the inset and is mirror-symmetric regarding the  $y$  axis. To generalise, this analysis of full angular dependence of the free energy of the two type particles has shown that each particle type has only one stable and no metastable equilibrium configurations, which is positive (and generally needed) for realisation of single multiparticle structures (colloidal crystals).

## 3 Results

### 3.1 Inter-particle potentials

The self-assembly of the colloidal particles depends crucially on their pair interaction potentials. The potentials for different mutual orientations and positions of type 1 and type 2 particles are presented in Fig. 4. Pair interactions between two type-1 particles are attractive along  $x$ ,  $y$  and also  $z$  direction, as evident from Fig. 4a. The calculated interaction between particles can be understood in view of the distortions in the sharp corners of the particles, especially the emergent surface boojum defects (see Fig. 3d and 3e). At particle surface to surface separations (displacement in Fig. 4) or order of magnitude larger than nematic correlation length the interaction is determined by the effective elasticity of the nematic, where the direct head-to-head approach between boojums leads to repulsion, whereas side approach leads to attraction, in line with works on interaction potential between e.g. spherical colloids with tangential anchoring. At separations of the order of nematic correlation length, the inter-particle interaction becomes determined by the nematic degree of order, where cores of the boojum defects or regions of low degree of order seek to fuse or overlap, in order to effectively reduce their volume, characterised by the energetically costly strong deformation. Indeed, this defect core-to-core interaction gives rise to rather strong binding potentials at short distances, which can be of the order of several  $100k_B T$ . Notably, the interaction poten-

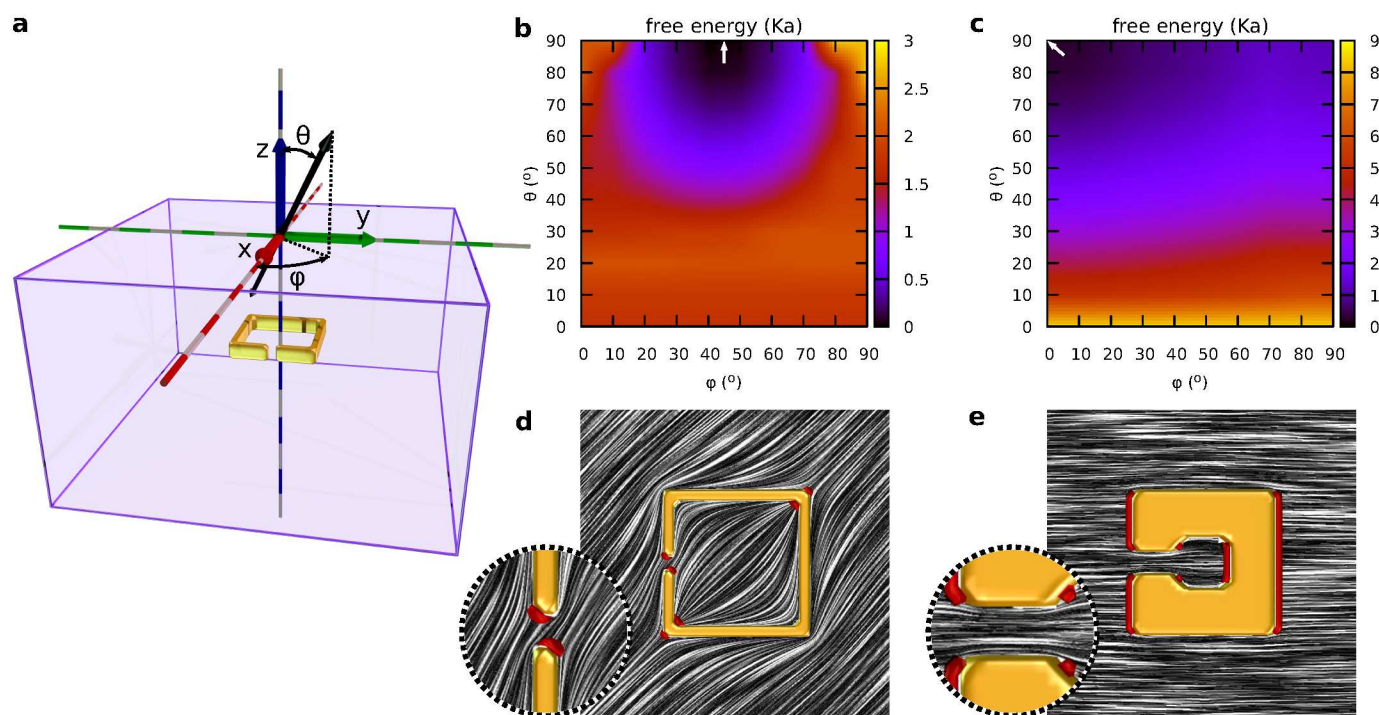


**Fig. 3 Preferential alignment of horseshoe particles.** (a) Scheme of the simulation box consisting of single particle in the centre of the box. The far-field nematic director, imposed at the walls of the simulation box (in purple), is indicated by black arrow and quantified with polar angles  $(\varphi, \theta)$ . Note that in order to simply the calculation, a different coordinate frame is used in this figure (as compared to e.g. Fig.1). (b) Type-1 particle has minimum of the free energy at  $\varphi = 45^\circ$ ,  $\theta = 90^\circ$ . (c) Type-2 particle has minimum of the free energy at  $\varphi = 0^\circ$ ,  $\theta = 90^\circ$ . (c),(d) The director field (illustrated in grayscale) and defects (red) around type-1 and type-2 particles, respectively. The insets show the director field in the slit. The defects are drawn as isosurfaces of nematic degree of order at  $S = 0.39$ . Free energy is given in units of  $Ka$ , where  $K$  is elastic constant in one elastic constant approximation and  $a$  is the size of the particle.

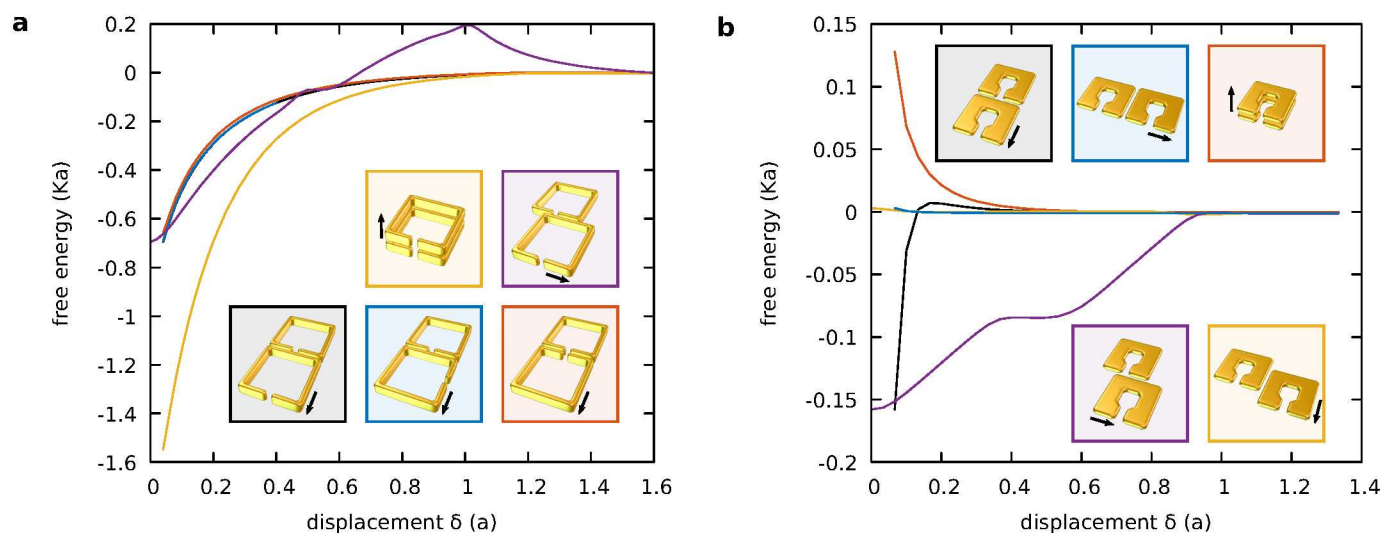


**Fig. 4 Pair interaction between horseshoe colloidal particles.** (a) Free energy of the two particles of type 1 in the nematic with far field direction at  $\varphi = 45^\circ$ ,  $\theta = 90^\circ$ . Free energy is reduced when particles get closer together, disregarding of the slit position, which is a sign of attractive interaction. (b) Free energy of type-2 particles is increased when the particles approach along axis  $y$  and  $z$  (blue and orange curves), which is a sign of repulsive interaction. Interaction between particles along axis  $x$  is still attractive. Displacement  $\delta$  between the particles is shown in units of their size  $a$ .

tial is attractive for directions for type 1 particles, but shows a repulsive direction for type 2 particles, despite the similar overall geometry of the particle shape. Therefore, results from Fig. 4 suggest that particle 1 is a good candidate for self-assembly –

and we will use it in the actual assembly of 2D and 3D crystals –, because of attractive interactions along all three particle interfaces, whereas the repulsive interactions between type-2 particles make it inappropriate for self-assembly beyond 1D chains.

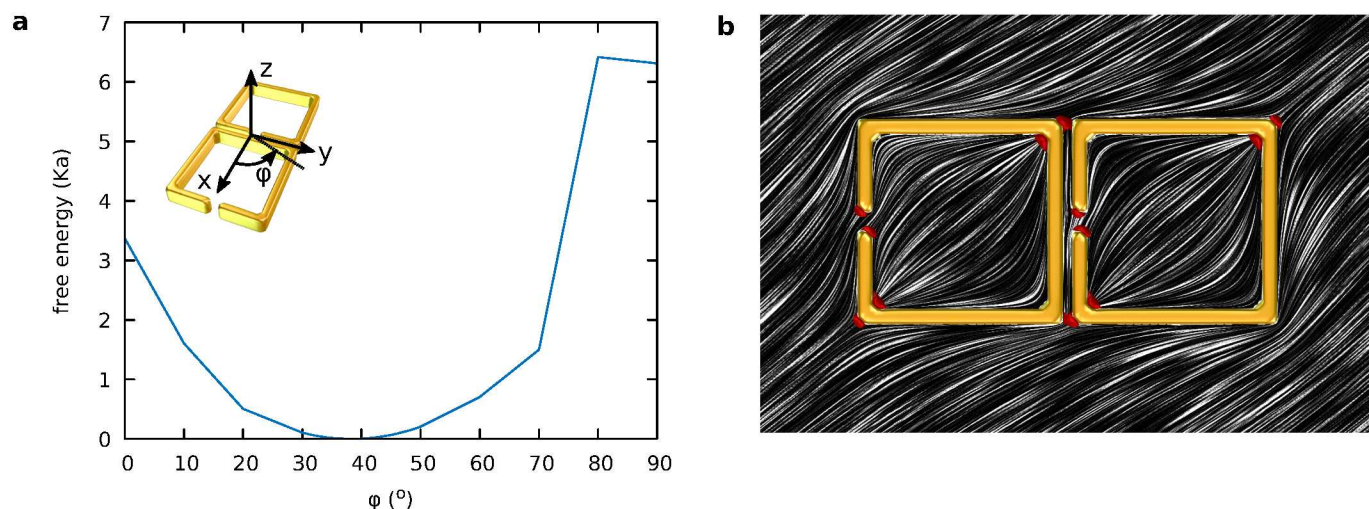


**Fig. 5** Equilibrium orientation of a bound pair of two horseshoe particles. (a) Free energy dependence of two-horseshoe dimer on the relative angle of the dimer with respect to the undistorted far field director. It is minimal at  $38^\circ$  ( $\theta$  is held at  $\pi/2$ ). (b) The stable bound pair of two horseshoe particles in nematic; director is shown with gray streamlines and defect regions in red.

More generally, this design of interaction potentials clearly shows that geometrical design and optimisation of exact particle shape (as here performed with extensive numerical simulations) can be used to broadly engineer interactions and self assembly in colloids of complex fluids, even reversing between repulsion and attraction directions.

The attractive interaction between two particles of type 1 causes them to stack together and form a dimer (Fig. 5b). Such two-horseshoe dimer performs as a single asymmetric particle of rectangular shape. Its asymmetry causes the shift of the free energy minimum to  $38^\circ$  (Fig. 5a); however, when the particle cluster restores its symmetry by introduction of a third particle, forming the V shape, the three-horseshoe particle cluster again exhibits its minimum at the  $45^\circ$ <sup>7</sup>. Notably, such reorientation is the result of the fact that self-assembly in nematic colloids generally is affected not only by effective pair-interactions between two particles but actually on multi-body contributions, as caused and transmitted via the long-range elasticity (softness) of the nematic orientational field. In view of this work, this multi-body effect is primarily seen in the restoration of torques in the structure, which clearly is of major importance for the self-assembly into larger particle structures.

### 3.2 2D nematic colloidal crystals from horseshoe particles

The attractive pair interaction functions of horseshoe particles of type 1 indicate that colloidal particles can undergo self-assembly and form stable 2D and even 3D colloidal crystals. We have examined the stability of 2D horseshoe colloidal crystal with simulations of single unit cell with periodic boundary conditions in both  $x$  and  $y$  direction, which is illustrated in Fig. 6a. The anchoring on the top and bottom confining cell walls is taken strong uniform planar at the angle  $\varphi = 45^\circ$  with regards to the  $x$ -axis, which was shown to be the optimum alignment direction of single colloidal particle (Fig. 3b). The displacement between the colloidal particles (illustrated on Fig. 6a) in both directions ( $\delta_x$

and  $\delta_y$ ) is varied by changing the unit cell size separately in  $x$  and  $y$  direction. Variations of lattice spacing affect the free energy as shown in Fig. 6b, where we see that increasing both displacements raises the free energy of the system, which implies that the 2D colloidal crystal of horseshoe particles is stable. Note that the dependence is symmetric regarding displacements in both  $x$  and  $y$  directions which is the consequence of similar pair interaction potentials (Fig. 4a). Fig. 6c shows the unit cell of colloidal crystal where both displacements are minimal and the structure is optimally stable with lowest free energy. The topological defects arise at all four corners of horseshoe particles, effectively binding the particles together via overlapping/sharing the regions of low nematic degree of order, i.e. the defect cores. The director field within the slit is asymmetric, as shown in the inset of Fig. 6c. Note that the director field between particles is predominantly parallel with the horseshoe particle frame, because of strong planar degenerate anchoring on the surfaces, but deforms in the region of the slit. Fig. 6d shows an illustration of the stable 2D horseshoe nematic colloidal crystal, with defects shown in red.

### 3.3 3D horseshoe nematic colloidal crystal

The stability of 3D nematic colloidal crystal of horseshoe particles was studied with simulations of single unit cell with periodic boundary conditions in all directions, as schematically illustrated in Fig. 7a. The initial direction of director field, initially set at the angle of  $\varphi = 45^\circ$  in the plane of the horseshoe, was preserved also after the relaxation. The displacements in all three directions  $\delta_x$ ,  $\delta_y$  and  $\delta_z$  are effectively varied by changing the unit cell size independently in all three directions. Variations of all three displacements affect the free energy as shown in Fig. 7b and 7c. When widening the displacements between the horseshoe colloidal particles in  $x$  and  $y$  direction we obtain an increase of the free energy of the colloidal crystal, similarly as in 2D colloidal crystal (Fig. 6), for displacement in  $z$ -direction  $\delta_z = 0.04a$ . The free energy is minimal at the point of smallest tested displace-

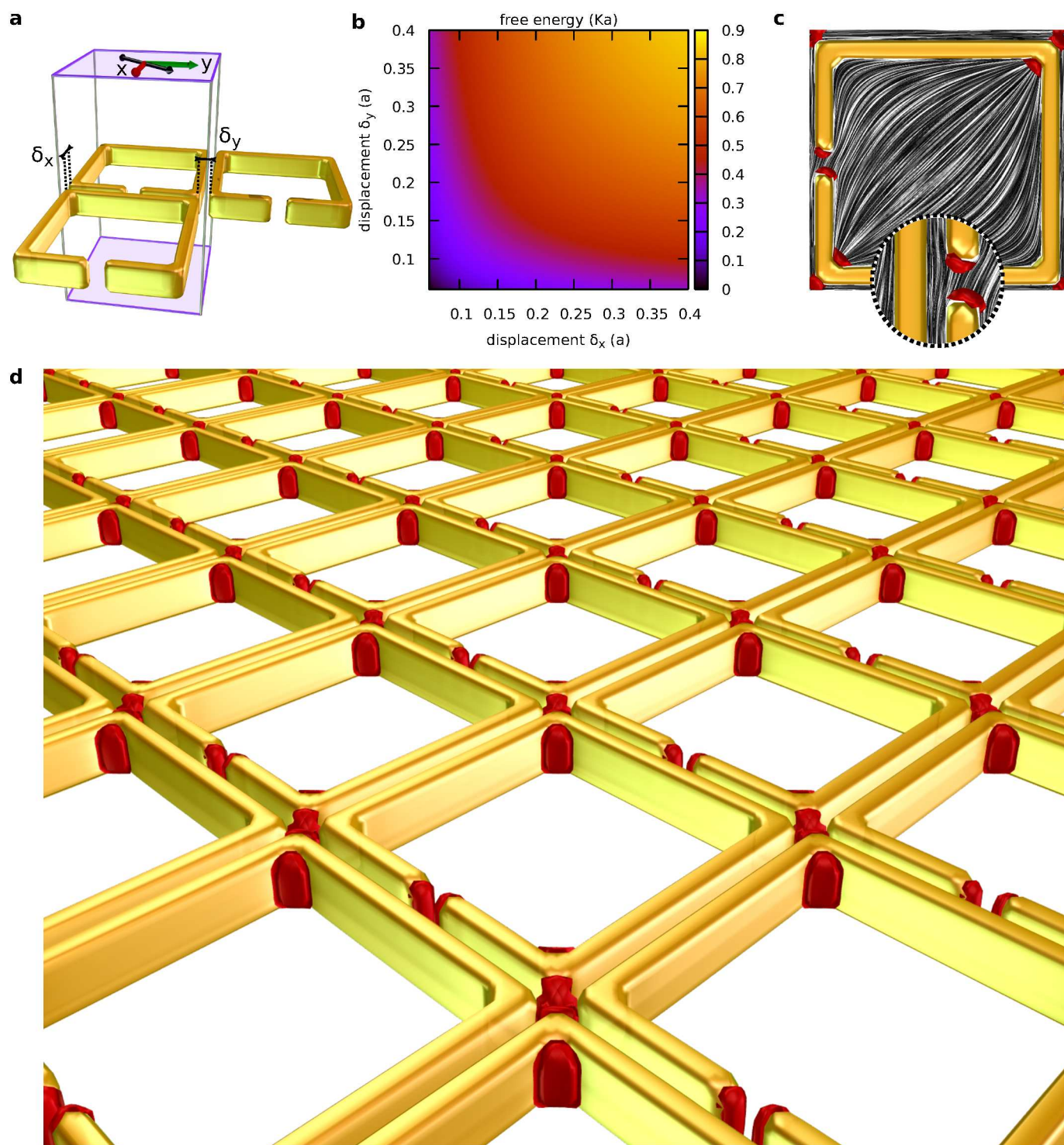


**Fig. 6 Two-dimensional horseshoe nematic colloidal crystal.** (a) Scheme of unit cell containing one horseshoe platelet with periodic boundary conditions at the cell sides in  $x$  and  $y$  direction and fixed anchoring, indicated with black arrow, at the cell walls (top and bottom in purple). Displacements  $\delta_x$  and  $\delta_y$  between the horseshoe colloidal particles are varied by changing unit cell size. (b) Free energy of the 2D horseshoe colloidal crystal varies with changing the displacements and is minimal for  $\delta_x = \delta_y = 0.04a$ . Free energy is measured in units of  $Ka$ , where  $K$  is elastic constant and  $a$  the size of horseshoe particle. (c) Horseshoe particle with the corresponding director field in one unit cell of the 2D colloidal crystal at optimal configuration. Inset shows the director field in the slit. (d) Illustration of multiple unit cells of the 2D colloidal crystal with defects depicted in red and equally oriented particle slits. Note that for the system shown, different mutual orientations of the slits are energetically similar, generally allowing for different slit orientations in the 2D colloidal crystals.

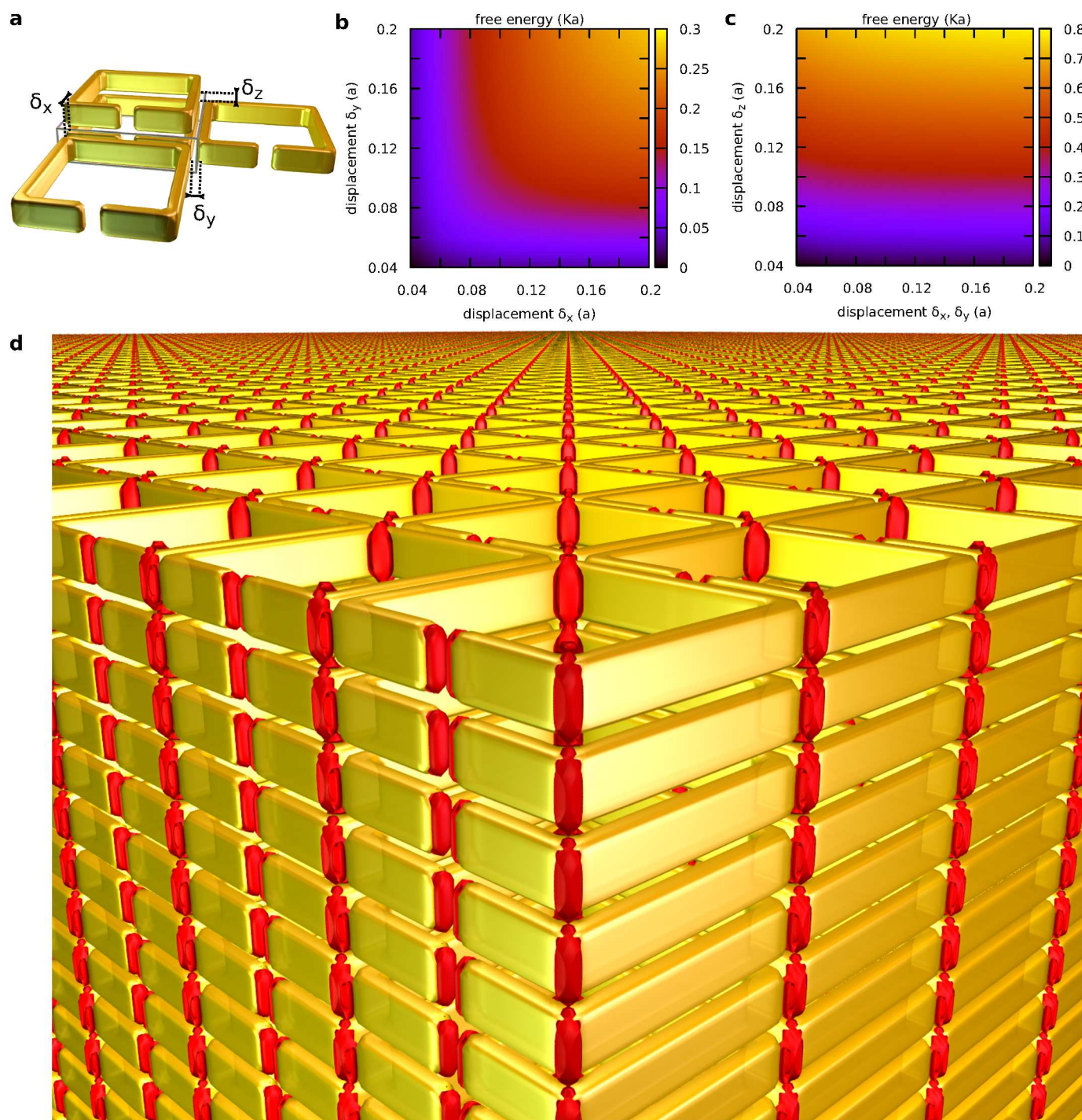


**Fig. 7** Three-dimensional horseshoe nematic colloidal crystal. (a) Scheme of unit cell of horseshoe colloidal crystal with periodic boundary conditions at all boundaries.  $\delta_x$ ,  $\delta_y$  and  $\delta_z$  shows displacements between nearest neighbours in all three directions. (b) Free energy of colloidal crystal dependent on variations of displacements  $\delta_x$  and  $\delta_y$ , with displacement  $\delta_z = 0.04a$  kept constant. (c) Free energy of colloidal crystal dependent on variations of  $\delta_x$  or  $\delta_y$  and  $\delta_z$  direction, with displacement  $\delta_y = 0.04a$  or  $\delta_x = 0.04a$  kept constant, respectively. Free energy of horseshoe colloidal crystal is minimal for displacements  $\delta_x = \delta_y = \delta_z = 0.04a$ . (d) Illustration of stable 3D horseshoe nematic colloidal crystal with topological defects depicted in red and equally oriented particle slits. Note that different mutual orientations of the slits are energetically similar, generally allowing for different slit orientations.

ments, which were  $\delta_x = \delta_y = 0.04a$ , where particles effectively get in contact, and short-range forces like steric and van der Waals (DLVO) would become of relevance but are not considered here. The free energy of the system shows also clear attraction along

the  $z$ -direction of the crystal. In Fig. 7c, we show the dependence of free energy of  $\delta_z$  versus  $\delta_x$ , with  $\delta_y$  being held constant at  $\delta_y = 0.04a$ , (note, which is equivalent to the dependence of  $\delta_z$  versus  $\delta_y$  with  $\delta_x = 0.04a$ ). Free energy is minimal at minimal

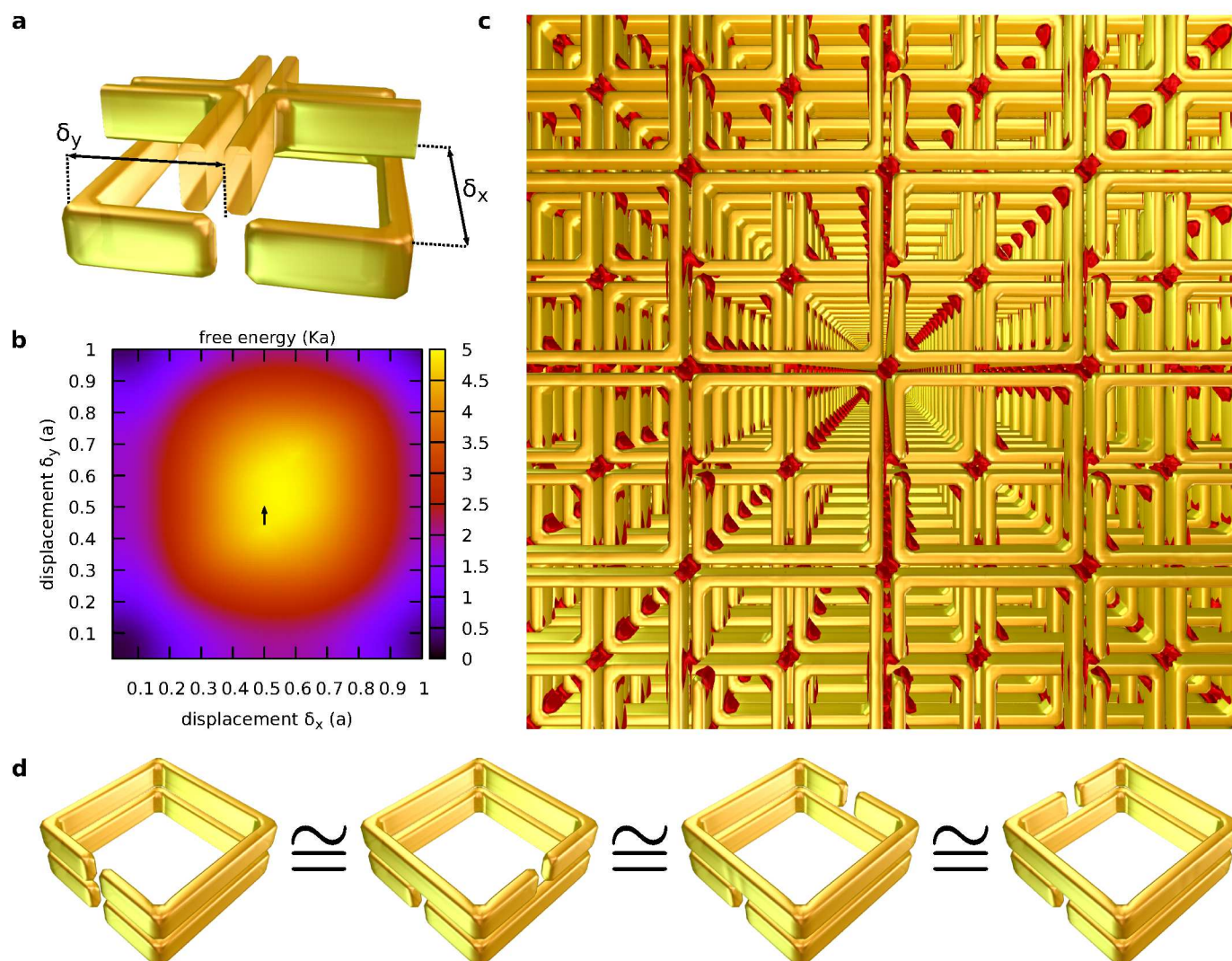


**Fig. 8 Stability of 3D horseshoe nematic colloidal crystal.** (a) Unit cell of a 3D colloidal crystal with two horseshoe particles stacked one above the other. The upper layer is shifted in both  $x$  and  $y$  direction. (b) The free energy of the 3D colloidal crystal with two shifted layers shown in (a). It is minimal for both displacements  $\delta_x = \delta_y = 0$ . (c) Illustration of the unstable colloidal crystal with half shifted layers (indicated with arrow on (b)), represents the unstable configuration. (d) The upper horseshoe in the unit cell is rotated relative to the bottom horseshoe particle. Specifically, anticlockwise rotation causes increase in the free energy for  $0.0018 Ka$ , which is small compared to other typical energy scales of the system. Similar order of magnitude increase in free energy emerges for other rotations.

simulated displacement  $\delta_z = 0.04a$ ). Free energy is presented here only in two complementary slices. However, the simulations were performed also at other configurations and show only one global minimum, which occurs when all three displacements are minimal  $\delta_x = \delta_y = \delta_z = 0.04a$ . This shows that 3D colloidal crystal constructed out of horseshoe building blocks is stable, forming a tetragonal crystal lattice. The stable 3D horseshoe nematic colloidal crystal is illustrated in Fig. 7d.

The stability of the 3D horseshoe colloidal crystal is further tested for any metastable configurations by including two horseshoe particles into the unit cell with periodic boundary conditions (Fig. 8a). This effectively creates a 3D colloidal crystal with two interchanging layers. First the upper particle is moved with respect to the lower, this effectively means that every second layer in the crystal is shifted to some extent in both  $x$  and  $y$  directions,

similar as shown in Fig. 8c. The free energy of such shifted colloidal crystals is represented in Fig. 8b and reveals the global minimum when  $\delta_x = \delta_y = 0$ . This is the configuration when lower and upper particle are perfectly aligned with each other, as shown already in Fig. 7. Fig. 8c shows the unstable configuration when both displacements are  $\delta_x = \delta_y = a/2$ . If the upper particle is rotated such that the slits are no longer aligned, the free energy of the system changes by less than  $0.0018 Ka$ , which is small compared to typical energy scales in the system (Fig. 8d). Therefore, overall, we show that horseshoe colloidal particles of type 1 do form a stable tetragonal colloidal crystal, shown in Fig. 7d. However, combined with the pair interaction functions nearly overlapping for relative orientations of  $0^\circ$  and  $90^\circ$  between the particles (see Fig. 4a), we see that the SRR particles in the assembled crystal most likely would not be oriented homogeneously, but could

be rotated by multiples of  $90^\circ$ . Indeed, from photonics perspective, this degeneracy in the particle slit orientations would affect the metamaterial response, especially to linearly polarised light, generally resulting in an effectively averaged response for the two slit orientations. For example, for individual particle, the optical response depends on the direction of the polarization of the incoming light relative to the slit orientation (for more see<sup>44</sup>), giving rise to different resonant behaviour. Therefore, having distributed orientations of the SRRs slits in 2D and 3D, would for already linearly polarised incoming light yield a generalised resonant behaviour with more possible excited resonant modes.

More generally, this work is part of a more general goal to be able to assemble colloids based on complex fluids, that can perform specific functions or material responses. In our case, the horseshoe particles – if metallic – can perform as effective LC (i.e. inductance L and capacitance C) resonators which is of direct relevance for light control with metamaterials<sup>31,44</sup>. Nevertheless, some principal distinct requirements for performance of the colloidal material (in our case the horseshoe shape of the particle) may turn out to be incompatible with the routes for the self-assembly. But the idea we demonstrate here is that – at least in systems of complex nematic fluid colloids – appropriate pre-design of colloidal objects may be used to affect and redesign the self-assembly, by changing both stability/metastability of equilibrium structures as well as the interaction potentials.

## 4 Conclusions

In this work, we demonstrate designed self-assembly of horseshoe colloidal crystals into 2D and 3D colloidal crystals, using numerical modelling based on Landau-de Gennes free energy minimisation. Distinctly, this work demonstrates the idea of geometrical pre-design of complex shaped – horseshoe – particles in nematic liquid crystal, to allow for assembly of 2D and 3D horseshoe nematic colloidal crystals for use as optical metamaterials building blocks. The key aims of the optimisation-design is to reduce possibilities (degrees of freedom) for the formation of various (irregular) strongly-bound metastable states, that commonly emerge in colloids of complex fluids, but are widely non-desired in photonic or optic applications. Using extensive computational optimisation of the preferential orientation of a single horseshoe particle in nematic liquid crystals based on its geometrical parameters, we show selection of two particle candidates for self assembly: one with relatively thin arms and small slit (type-1) which orients at an angle of  $45^\circ$  with respect to the nematic director, and one with relatively thick arms (type-2 particle), which aligns with the director. For these two particle candidates we then examine the anisotropic interparticle pair interaction potentials, which is then used to finalise the selection of the particle geometry for the assembly. Indeed, using type-1 particles, we demonstrate formation of stable 2D and 3D horseshoe nematic colloidal crystals. Interestingly, the particles are mutually effectively glued (bound) by shared regions of reduced degree of order, i.e. cores of surface induced topological defects. The potential of self-assembly makes the demonstrated structures interesting for various applications, most notably for photonic metamaterial applications, where elements with a slit are used to produce resonances in the magnetic

field.

## Acknowledgements

Authors acknowledge funding from Slovenian Research Agency grants (P1-0099, J1-7300, L1-8135), MIZS research Early career researcher 2.1 grant and USAF AFRL EOARD research project Nematic Colloidal Tilings as Tunable Soft Metamaterials (grant no. FA9550-15-1-0418).

## References

- 1 C. Blanc, D. Coursault and E. Lacaze, *Liquid Crystals Reviews*, 2013, **1**, 83.
- 2 H. K. Bisoyi and S. Kumar, *Chem. Soc. Rev.*, 2011, **40**, 306.
- 3 I. Muševič, *Liquid Crystal Colloids*, Springer International Publishing, New York, 2017.
- 4 J. P. F. Lagerwaal, *Liquid Crystals with Nano and Microparticles*, World Scientific, 2016.
- 5 T. Hegmann, H. Qi and V. M. Marx, *J Inorg Organomet Polym*, 2007, **17**, 483.
- 6 G. M. Whitesides, *Science*, 2002, **295**, 2418.
- 7 C. P. Lapointe, T. G. Mason and I. I. Smalyukh, *Science*, 2009, **326**, 1083.
- 8 I. Smalyukh, O. Lavrentovich, A. Kuzmin, A. Kachynski and P. Prasad, *Phys. Rev. Lett.*, 2005, **95**, 157801.
- 9 H. Stark, *Phys. Rep.*, 2001, **351**, 387.
- 10 J.-C. Loudet, P. Barois and P. Poulin, *Nature*, 2000, **407**, 611.
- 11 I. Muševič, M. Škarabot, U. Tkalec, M. Ravnik and S. Žumer, *Science*, 2006, **313**, 954.
- 12 K. Sentker, A. W. Zantop, M. Lippmann, T. Hofmann, O. H. Seeck, A. V. Kityk, A. Yildirim, A. Schönhals, M. G. Mazza and P. Huber, *Phys. Rev. Lett.*, 2018, **120**, 067801.
- 13 M. Ravnik, G. P. Alexander, J. M. Yeomans and S. Žumer, *Proc. Natl. Acad. Sci.*, 2011, **108**, 5188.
- 14 G.-R. Yi, D. J. Pine and S. Sacanna, *J. Phys.: Condens. Matter*, 2013, **25**, 193101.
- 15 H. Yoshida, K. Asakura, J. Fukuda and M. Ozaki, *Nat. Commun.*, 2015, **6**, 7180.
- 16 Y. Li, E. Prince, S. Cho, A. Salari, Y. M. Golestani, O. D. Lavrentovich and E. Kumacheva, *Proc. Natl. Acad. Sci.*, 2017, **114**, 2137.
- 17 N. V. Solodkov, J. uk Shim and J. C. Jones, *Nat. Commun.*, 2019, **10**, 14256.
- 18 B. Senyuk, Q. Liu, S. He, R. D. Kamien, R. B. Kusner, T. C. Lubensky and I. I. Smalyukh, *Nature*, 2013, **493**, 200.
- 19 N. M. Silvestre and M. Tasinkevych, *Phys. Rev. E*, 2017, **95**, 012606.
- 20 J. Dontabhaktuni, M. Ravnik and S. Žumer, *Proc. Natl. Acad. Sci.*, 2014, **111**, 2464.
- 21 T. C. Lubensky, D. Pettey, N. Currier and H. Stark, *Phys. Rev. E*, 1998, **57**, 610.
- 22 U. M. Ognysta, A. B. Nych, V. A. Uzunova, V. M. Pergamenschik, V. G. Nazarenko, M. Škarabot and I. Muševič, *Phys. Rev. E*, 2011, **83**, 041709.
- 23 Z. Eskandari, N. M. Silvestre and M. M. T. da Gama, *Lang-*

- muir*, 2013, **29**, 10360.
- 24 S. Püschel-Schlotthauer, T. Stieger, M. Melle, M. G. Mazza and M. Schoen, *Soft Matter*, 2016, **12**, 469.
- 25 I. I. Smalyukh, *Annu. Rev. Condens. Matter Phys.*, 2018, **9**, 207.
- 26 A. B. Golovin and O. D. Lavrentovich, *Applied Physics Letters*, 2009, **95**, 254104.
- 27 Y. J. Cha, D. S. Kim and D. K. Yoon, *Adv. Funct. Mater.*, 2017, **27**, 1703790.
- 28 E. Lee, Y. Xia, R. C. Ferrier, H.-N. Kim, M. A. Gharbi, K. J. Stebe, R. D. Kamien, R. J. Composto and S. Yang, *Adv. Mater.*, 2016, **28**, 2731.
- 29 M. Draper, I. M. Saez, S. J. Cowling, P. Gai, B. Heinrich, B. Donnio, D. Guillon and J. W. Goodby, *Adv. Funct. Mater.*, 2011, **21**, 1260.
- 30 D. R. Smith, W. J. Padilla, D. C. Vier, S. C. Nemat-Nasser and S. Schultz, *Phys. Rev. Lett.*, 2000, **84**, 4184.
- 31 N. I. Zheludev and Y. S. Kivshar, *Nat. Mater.*, 2012, **11**, 917.
- 32 J. Aplinc, M. Štimulak, S. Čopar and M. Ravnik, *Liq. Cryst.*, 2016, **43**, 2320.
- 33 Q. Liu, Y. Yuan and I. I. Smalyukh, *Nano Lett.*, 2014, **14**, 4071.
- 34 D. C. Zografopoulos, R. Asquini, E. E. Kriezis, A. d'Alessandro and R. Beccherelli, *Lab Chip*, 2012, **12**, 3598.
- 35 J. Fontana, G. K. B. da Costa, J. M. Pereira, J. Naciri, B. R. Ratna, P. Palfy-Muhoray and I. C. S. Carvalho, *Appl. Phys. Lett.*, 2016, **108**, 081904.
- 36 K. Yoshino, Y. Shimoda, Y. Kawagishi, K. Nakayama and M. Ozaki, *Appl. Phys. Lett.*, 1999, **75**, 932.
- 37 K. Busch and S. John, *Phys. Rev. Lett.*, 1999, **83**, 967.
- 38 J. B. Pendry, A. J. Holden, W. J. Stewart and I. Youngs, *Phys. Rev. Lett.*, 1996, **76**, 4773.
- 39 R. A. Shelby, *Science*, 2001, **292**, 77.
- 40 B. Atorf, T. Funck, T. Hegmann, S. Kempter, T. Liedl, K. Martens, H. Mühlenbernd, T. Zentgraf, B. Zhang, H. Kitzrow and M. Urbanski, *Liq. Cryst.*, 2017, **44**, 1.
- 41 P. G. de Gennes and J. Prost, *The physics of liquid crystals*, Oxford University Press, Oxford, 1993.
- 42 J.-B. Fournier and P. Galatola, *Europhys. Lett.*, 2005, **72**, 403.
- 43 M. Ravnik and S. Žumer, *Liq. Cryst.*, 2009, **36**, 1201.
- 44 A. Pusovnik, J. Aplinc and M. Ravnik, *Sci. Rep.*, 2019, **9**, 7025.
- 45 K. Stratford, O. Henrich, J. S. Lintuvuori, M. E. Cates and D. Marenduzzo, *Nat. Commun.*, 2014, **5**, 3954.
- 46 K. P. Zuhail and S. Dhara, *Soft Matter*, 2016, **12**, 6812.
- 47 N. Wang, J. S. Evans, Q. Liu, S. Wang, I.-C. Khoo and S. He, *Opt. Mater. Express*, 2015, **5**, 1065.
- 48 M. Yada, J. Yamamoto and H. Yokoyama, *Phys. Rev. Lett.*, 2004, **92**, 185501.
- 49 A. Nych, U. Ognysta, M. Škarabot, M. Ravnik, S. Žumer and I. Muševič, *Nat. Commun.*, 2013, **4**, 1489.
- 50 Y. Tamura and Y. Kimura, *Soft Matter*, 2016, **12**, 6817.
- 51 Y. Yuan, G. N. Abuhaimeed, Q. Liu and I. I. Smalyukh, *Nat. Commun.*, 2018, **9**, 10081.
- 52 Y. Luo, D. A. Beller, G. Boniello, F. Serra and K. J. Stebe, *Nat. Commun.*, 2018, **9**, 1253751.
- 53 X. Li, J. C. Armas-Pérez, J. P. Hernández-Ortiz, C. G. Arges, X. Liu, J. A. Martínez-González, L. E. Ocola, C. Bishop, H. Xie, J. J. de Pablo and P. F. Nealey, *ACS Nano*, 2017, **11**, 6492.
- 54 A. V. Straube, J. M. Pagès, A. Ortiz-Ambriz, P. Tierno, J. Ignés-Mullol and F. Sagués, *New J. Phys.*, 2018, **20**, 075006.
- 55 G. E. Volovik and O. D. Lavrentovich, *Zh. Eksp. Teor. Fiz.*, 1983, **85**, 1159.
- 56 M. Tasinkevych, N. M. Silvestre and M. M. T. da Gama, *New J. Phys.*, 2012, **14**, 073030.
- 57 A. Martinez, L. Hermosillo, M. Tasinkevych and I. I. Smalyukh, *Proc. Natl. Acad. Sci.*, 2015, **112**, 4546.